Controlled Hypersonic Flight
Air Data System and Flight Instrumentation

Georg Koppenwallner
HTG Hyperschall Technology Göttingen
Max-Planck-Strasse 19
37191 Katlenburg-Lindau, Germany

Summary
The main task of an air data system, namely to deduce from measurement on the body the aerodynamic free stream conditions will be outlined. Emphasis will also be given to the limitations of aerodynamic systems.
A short review of the aerodynamic probe functions relating measured quantities to the desired free stream conditions and vehicle orientation will be given.
After explaining the principle elements of an air data system the design of individual components will be outlined.
The design of an air data system depends strongly on the flight envelope, re-entry trajectory and vehicle structure. Flight envelope and re-entry trajectory influence primarily the sensor range and sensor head design. Vehicle structure has a strong influence on the probe installment.
The principal components are: Probe heads, probe mounting elements, sensors, sensor electronics, harness and data acquisition system.
In a similar way the design of calorimetric heat flux sensors will be explained.
Testing and flight qualification are one of the mayor efforts during development of an air data system and flight instrumentation. Therefore the principal steps for these activities will also be outlined.

Paper presented at the RTO AVT Lecture Series on "Critical Technologies for Hypersonic Vehicle Development", held at the von Kármán Institute, Rhode-St-Genèse, Belgium, 10-14 May, 2004, and published in RTO-EN-AVT-116.

Content

1. Introduction

Air data systems have to provide information on the ambient air and on the vehicle state of flight relative to ambient air. For an operational vehicle these state quantities are important for the vehicle control and guidance. For an experimental research vehicle these quantities are necessary for reduction of quantities measured on the vehicle itself. Thus the air data system should in combination with other on board or remote measurement quantify the state of the ambient atmosphere and the state of the vehicle. Typical supplementary onboard or remote measurements are acceleration vector sensing and radar tracking.

2. Tasks and requirement and of an air data system

2.1 Air data system tasks.

Air data systems have in general a specific task and they have in addition to comply with a set of requirements [1].
The main task concerns information on ambient air and on the vehicle state as outlined below.

Information on ambient atmosphere

As the main aerodynamic re-entry occurs in the homosphere (H < 120 km) with constant molecular mass we need only 2 quantities to determine the atmospheric state, pressure p, density ρ, and temperature T. For H < 120 km the molecular mass is constant with a value of M = 28.96 kg/kmol.

Information on vehicles aerodynamic state

Vehicles aerodynamic state is in principle determined by the flight velocity vector relative to ambient air in a body fixed coordinate system. This requires the determination of the three scalar quantities.
In principle this measurement is achieved by determination of magnitude of velocity V and the aerodynamic angle of attack α and the angle of side slip β.
In summary one needs 5 combinations of quantities in order to completely describe the vehicles state in an aerodynamic reference plane

Quantity	
1 Free stream dynamic pressure	$q = (\rho/2)V^2$
2 Angles of attack	α
3 Angle of sideslip	β
4 Free stream pressure or temperature	p or T
5 Flight velocity or density	V or ρ

In a flush mounted Air Data System (FADS) the vehicle itself acts as an aerodynamic probe. Thus one has to relate physical quantities measured at the vehicle surface to the atmospheric free stream and to the vehicle's velocity and aerodynamic orientation. Fig. 1 shows that the atmospheric free stream and the vehicle flow field determine the local surface properties.

$$p(\text{surface}) = \text{Function}\ (V, \rho, T, \alpha, \beta, \text{vehicle shape, location})$$

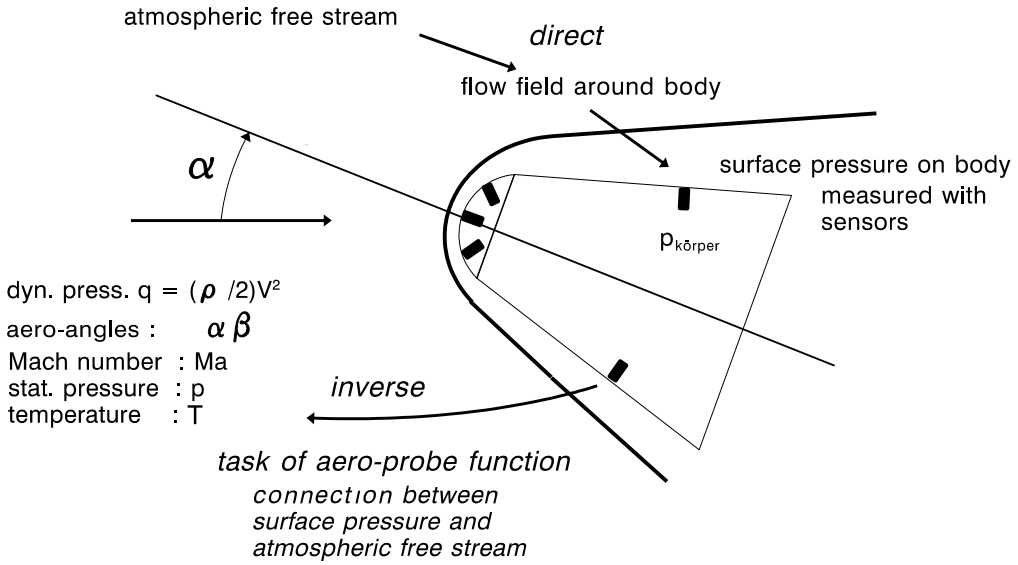

Fig.1. The main tasks of an aerodynamic air-data system
(inverse problem has to be solved)

Fig. 1: The main tasks of an aerodynamic air data system

A flush mounted air data system has, however, to solve the inverse problem, namely to deduce from a surface measurement the state of the atmosphere and the vehicle orientation. The solution of this inverse problem is by nature much more complex because one identical surface quantity can result from a variety of free-stream conditions and vehicle orientations. In order to find the unique inverse solution, a set of surface quantities have to be measured. From this set of measurements the compatible solutions have to be isolated in order to obtain a unique solution for the free stream quantity.

2.2 Air data system requirements

The requirements may be split up in mission dependent, operational and vehicle specific.

Mission dependent requirements

a. Altitude and velocity range of mission to be covered
b. Accuracy, response time
c. Availability of evaluated information (Immediately as input for flight control after flight for reconstruction of aerodynamic environment)

Operational requirements

a. Heat loads (mainly for sensor heads)
b. Dynamic, vibration loads (sensors and electronics)
a. Response time

Vehicle dependent requirements

a. Location for installation
b. Compatibility with vehicles external internal structure

3. The aerodynamic probe functions

The aerodynamic probe functions establish relations between the measured quantity of the sensor head (in our case surface pressure) and the aerodynamic free stream quantities. This is mathematically an inverse problem, which only in simple cases can be solved directly. In order to simplify the situation we select as representative vehicle shape a blunted cone similar to EXPERT [2] and restrict the analysis to the hypersonic part of the re-entry regime.

3.1 Free-stream dynamic pressure determination at Ma >>1

Free stream dynamic pressure should be determined with a pressure port installed in the vehicles nose. We then can use the classical Raleigh-Pitot relation [3] given below.

$$\frac{P_{t,2}}{p_1} = \left(\frac{\kappa+1}{2} Ma_1^{\,2}\right)^{\kappa/(\kappa-1)} \left(\frac{\kappa+1}{2\kappa Ma_1^{\,2} - (\kappa-1)}\right)^{1/(\kappa-1)}$$

with $\frac{q_1}{p_1} = \frac{2}{\kappa} Ma_1^2$ and $q_1 = \frac{\rho_1}{2} V_1^2$ we obtain:

$$\frac{P_{t,2}}{q_1} = \frac{2}{\kappa}\frac{1}{Ma_1^2}\left(\frac{\kappa+1}{2} Ma_1^2\right)^{\kappa/(\kappa-1)} \left(\frac{\kappa+1}{2\kappa Ma_1^2 - (\kappa-1)}\right)^{1/(\kappa-1)}$$

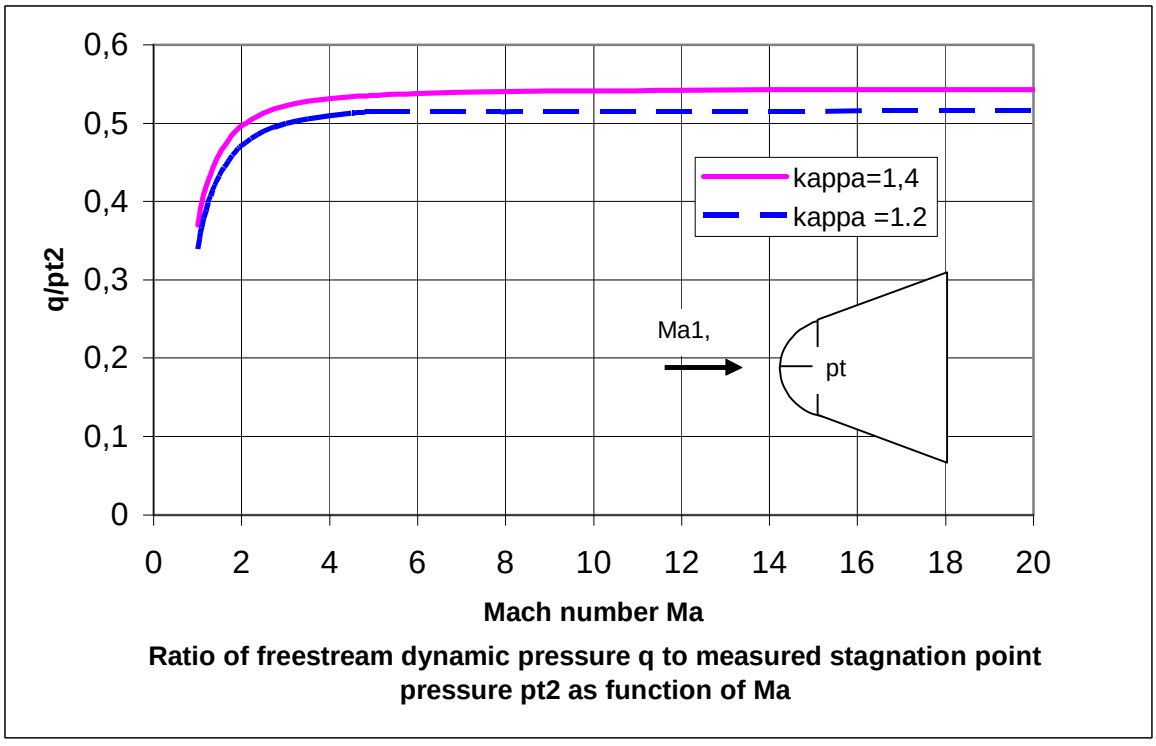

Fig. 2: Ratio of free stream dynamic to Pitot pressure as function of Mach number

Fig. 2 shows the ratio of actual free stream dynamic pressure to measured Pitot pressure as function of Mach number Ma. It is evident that for Ma > 4 this pressure ratio becomes independent from Ma. Thus the free stream dynamic pressure can directly be determined by the measured Pitot pressure. It is also important to note that real gas effects have only a minor influence on the stagnation point pressure. Equilibrium chemistry [4] reduces the q/pt2 ratio from q/pt2 = 0.54 for κ= 1.4 to a value of q/pt2 = 0.52 which corresponds to κ=1.2.

3.2 Mach number Ma and static pressure determination for Ma >> 1

Mach number determination requires beside of the Pitot pressure also a static pressure determination. For our test case vehicle this can only be done on the lateral conical surface.

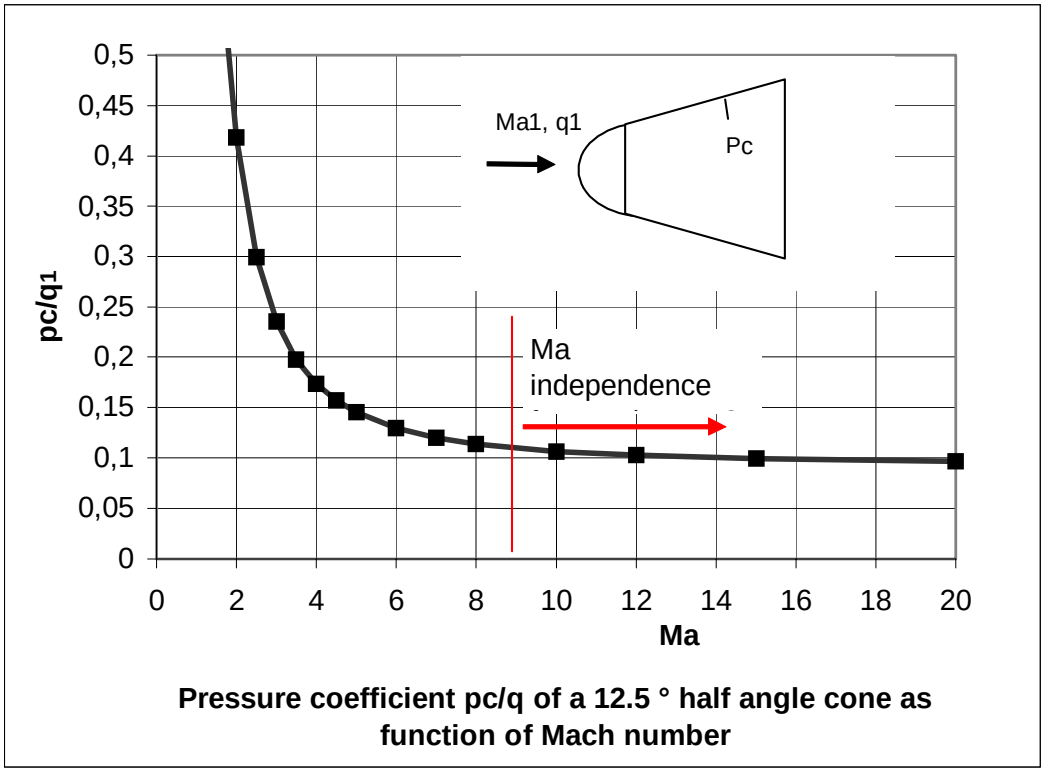

Pressure coefficient pc/q of a 12.5 ° half angle cone as function of Mach number

Fig. 3: Pressure coefficient of a 12.5° half angle cone and Mach number independence

In Fig. 3 we show the pressure coefficient of a cone half angle Θ = 12.5 ° as function of Mach number. It is evident that due to the hypersonic Mach number independence principle, which holds also for slender bodies with Ma *sin θ >2 the cone pressure is only a function of the free stream dynamic pressure and the cone angle. We therefore can not use the combination of Pitot and cone pressure in order to determine the free stream Mach number because both quantities are only functions of the free stream dynamic pressure q. For angle of attack and angle of sideslip determination the Mach number independence principle can however be used to derive simple analytic expressions.

3.3 Flight Wind angles and basic considerations

The definition of the US standard aerodynamic coordinate system [5] and the corresponding angle of attack α and side slip β are used in the following.

The Newtonian impact method states, that the local surface pressure depends only on the angle Θ between local surface normal and free stream vector as shown below.

$$p(\Theta) = p(\Theta = 0°) \cdot \cos^2 \Theta \qquad \text{for } -90° < \Theta < 90°$$
$$p(\Theta) = 0 \qquad \text{for } 90° < \Theta < 270°$$

Newtonian method is an acceptable approximation for $Ma \cdot \cos(\Theta) > 2$.

We analyze the probe function for 5 sensors installed in an axis symmetric body with a blunt nose. The following Table shows in a general way the angles φ and θ defining the installation conditions of the five probes.

Fig 4 explains for an axis-symmetric body the sensor installation angles and the flight wind angles α, β. In order to achieve a simple formulation for the probe functions a symmetric installation with $\theta_1 = \theta_2 = \theta_3 = \theta_4 = \theta$ will be used for the following analysis.

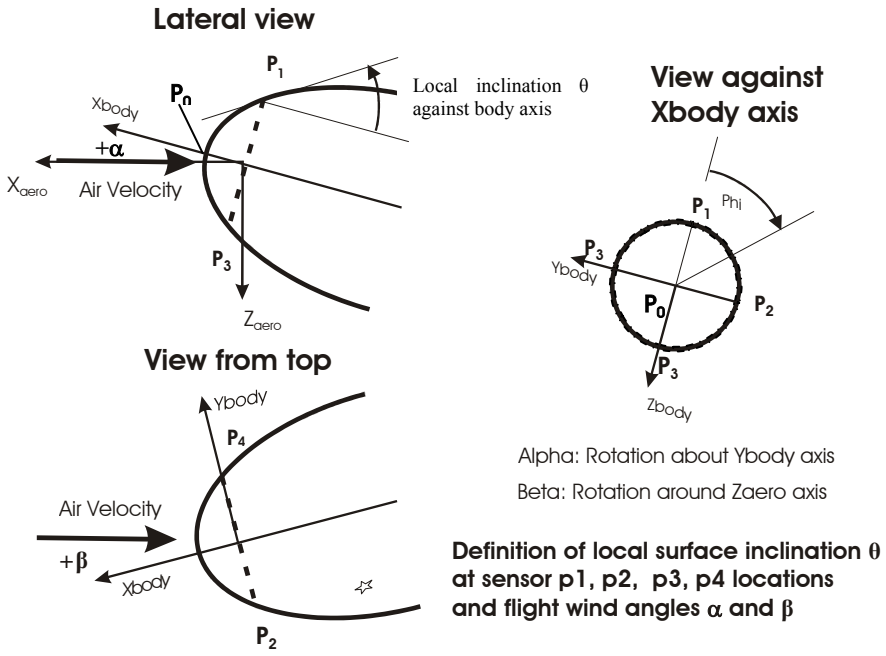

Fig. 4: Definition of local surface inclination and flight wind angles

No.	Pressure	Probe	Circumference Angle ϕ [°]	Local surface inclination θ against body x axis
0	P_0	Stagn. Point	0	$\theta = 90°$
1	P_1	Alpha 1	$\phi_1 = 0$	θ_1
2	P_2	Beta 1	$\phi_2 = 90$	θ_2
3	P_3	Alpha 2	$\phi_2 = 180$	θ_3
4	P_4	Beta 2	$\phi_4 = 270$	θ_4

Table 1: Conditions for sensor installation

In the NASA TR-R-127 [6] formula for the 'Newtonian' pressure distribution on axis-symmetric bodies in dependence of the flight wind angles are presented.
The circumferential pressure distribution of a general axis-symmetric body is given as function of flight wind angles α, β and the local angles of inclination θ and circumference ϕ.

$$cp = k_N(\sin\theta\cos\alpha\cos\beta - \cos\theta\sin\phi\sin\beta - \cos\phi sos\theta\sin\alpha\cos\beta)^2$$

For the spherical stagnation point the following expression holds

$$cp_0 = k_N(\cos\alpha\cos\beta)^2$$

with k_N given by $k_N = \dfrac{\kappa+3}{\kappa+1}$ for modified Newtonian theory.
Based on this formula simple probe functions have been derived in [1] which are shortly outlined below

3.4 Derivation of α, β sensor functions

For a symmetric circumferential installation of 5 pressure probes the angular functions cos ϕ and sin ϕ have values as shown in the following table

No	Pressure	Probe	Circumference Angle ϕ [°]	Cos ϕ	Sin ϕ
0	P_0	Stagn. Point	0		
1	P_1	Alpha 1	$\phi_1 = 0$	1	0
2	P_2	Beta 1	$\phi_2 = 90$	0	1
3	P_3	Alpha 2	$\phi_2 = 180$	-1	0
4	P_4	Beta 2	$\phi_4 = 270$	0	-1

Table 2: Pressure probe installation on blunted axis symmetric body

Using these values one obtains for the Alpha 1, Alpha 3, Beta 2 and Beta 4 sensors the following pressure formula set:

$$cp(\text{Alpha 1}) = k_N\cos^2\beta(\sin\theta\cos\alpha - \cos\theta\sin\alpha)^2$$
$$cp(\text{Alpha 3}) = k_N\cos^2\beta(\sin\theta\cos\alpha + \cos\theta\sin\alpha)^2$$
$$cp(\text{Beta 2}) = k_N(\sin\theta\cos\alpha\cos\beta - \cos\theta\sin\beta)^2$$
$$cp(\text{Beta 4}) = k_N(\sin\theta\cos\alpha\cos\beta + \cos\theta\sin\beta)^2$$

These four equations have to be solved in order to determine with the 4 measured pressures the two flight wind angles α, β.
The solution procedure can substantially be simplified when the probe positions are selected at local surface inclination with θ = 45°. We then have sin 45° = cos 45° and the equations are further simplified to

$$cp(\text{Alpha 1}) = k_N \sin^2 45° \cos^2 \beta (\cos\alpha - \sin\alpha)^2$$
$$cp(\text{Alpha 3}) = k_N \sin^2 45° \cos^2 \beta (\cos\alpha + \sin\alpha)^2$$
$$cp(\text{Beta 2}) = k_N \sin^2 45° (\cos\alpha \cos\beta - \sin\beta)^2$$
$$cp(\text{Beta 4}) = k_N \sin^2 45° (\cos\alpha \cos\beta + \sin\beta)^2$$

For the differential pressures $\Delta cp(\text{Alpha 3 - Alpha 1})$ and $\Delta cp(\text{Beta 4 - Beta 2})$ we obtain:

$$\Delta cp(\text{Alpha 3 - Alpha 1}) = k_N 4 \sin^2 45° \cos^2 \beta \cos\alpha \sin\alpha$$
$$\Delta cp(\text{Beta 4 - Beta 2}) = k_N 4 \sin^2 45° \cos\beta \sin\beta \cos\alpha$$

We arrive at an explicit solution if we normalize the above equations by the geometric stagnation point values cp_0. The beta dependence in the alpha formula is then compensated by the stagnation point pressure.

$$\frac{\Delta cp(\text{Alpha 3 - Alpha 1})}{cp_0} = \frac{k_N 4 \sin^2 45° \cos^2 \beta \cos\alpha \sin\alpha}{k_N \cos^2 \beta \cos^2 \alpha} = 4 \sin^2 45° * \tan\alpha$$
$$\frac{\Delta cp(\text{Beta 4 - Beta 2})}{cp_0} = \frac{k_N 4 \sin^2 45° \cos\beta \sin\beta \cos\alpha}{k_N \cos^2 \beta \cos^2 \alpha} = 4 \sin^2 45° \frac{\tan\beta}{\cos\alpha}$$

We note that due to the normalization with cp_0 the Newton factor k_N and the dynamic pressure are eliminated from the functions and we obtain as final probe functions:

$$\alpha = \arctan\left(\frac{1}{4 \sin^2 45°} \frac{(p3 - p1)}{p_0}\right)$$
$$\beta = \arctan\left(\frac{\cos\alpha}{4 \sin^2 45°} \frac{(p4 - p2)}{p_0}\right)$$

The angle of attack α can now directly determined by the measured pressure ratio $(cp3 - cp1)/cp0$ and in a second step the sideslip angle β can be determined with $(cp4 - cp2)/cp0$. It is evident that there exists only a small influence of alpha on the beta pressure ratio function.

Fig. 5 and Fig. 6 show the alpha pressure ratio $(p3 - p1)/p0$ and the beta pressure ratio $(p4 - p2)/p0$ as function of the corresponding angles. It should be noted that the formula are only valid for $\alpha < 45°$ and $\beta < 45°$. For $\alpha > 45°$ or $\beta > 45°$ the sensors will move into the shadowed flow regime with p=0, a situation which in the above derivation has not been considered.

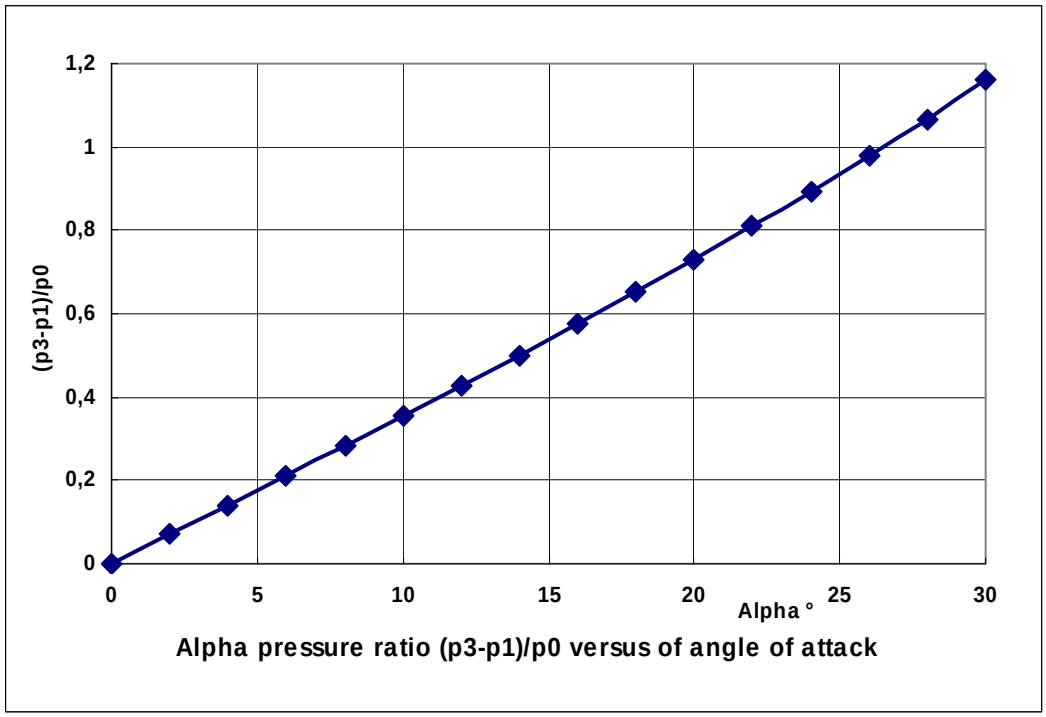

Fig. 5: Alpha pressure ratio p3-p1/p0 versus angle of attack, Newtonian pressure law, Sensor installation at θ = 45°

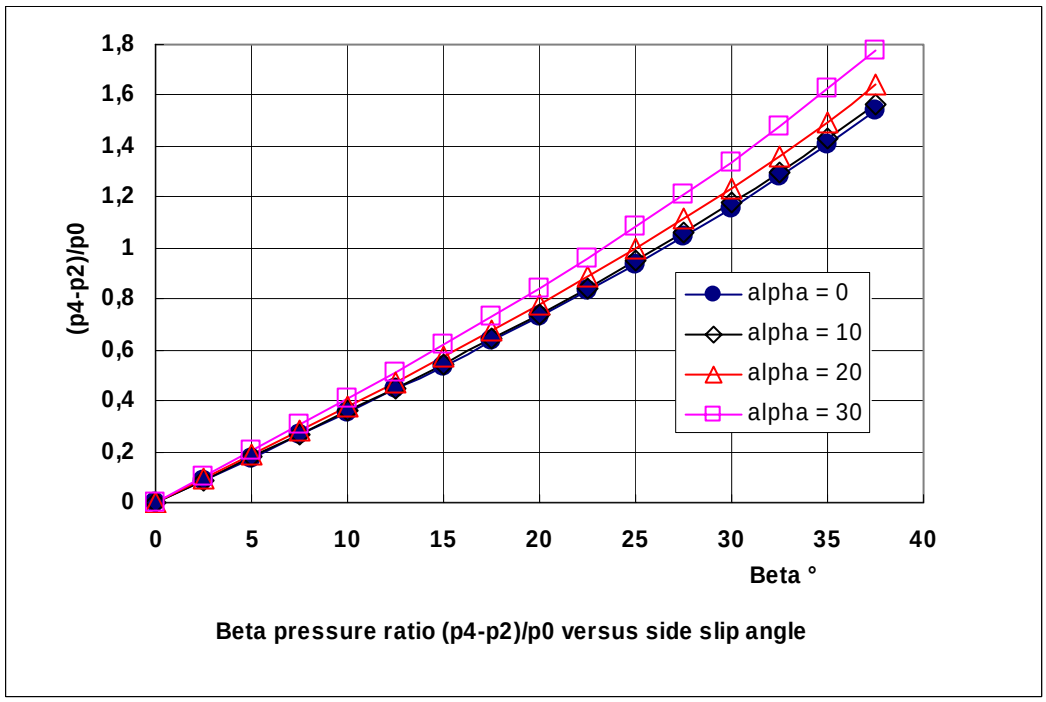

Fig. 6: Beta pressure ratio p4-p2/p0 versus angle of attack, Newtonian pressure law, Sensor installation at θ = 45°

In a CFD study [7] conducted at CLE with Navier-Stokes codes the above analytical formulation has been tested for EXPERT [2] vehicle conditions along the entry trajectory. It was found that viscous boundary and real gas effects have only a minor influence on the analytical derived probe functions for Mach numbers Ma> 5.
Based on this study small correction terms for the probe functions, which amount to about 6%, have been developed by CLE.

3.5 Sensitivity and error analysis

For primary importance for the directional sensitivity of one pressure sensing orifice is the local inclination Θ. Newtonian pressure is given by $p/p(\Theta=0) = \cos^2\Theta$. Taking the derivative $d(p/p_0)/d\Theta$ we obtain:

$$\frac{d(p/po)}{d\Theta} = -2\cos\Theta\cdot\sin\Theta$$

Fig. 7 shows for one pressure tap the Newtonian pressure and the directional sensitivity. It is evident that the sensor installation at Θ = 45° provides the largest directional sensitivity. In blunt capsule like bodies of the Apollo and ARD type only a very small angular sensitivity can be achieved.
Thus the selected pressure port locations with Θ = 45° and Δϕ = 90 ° are the optimum positions for flight wind angle determination. This special angular arrangement provides not only an explicit probe function but also the highest angular resolution.

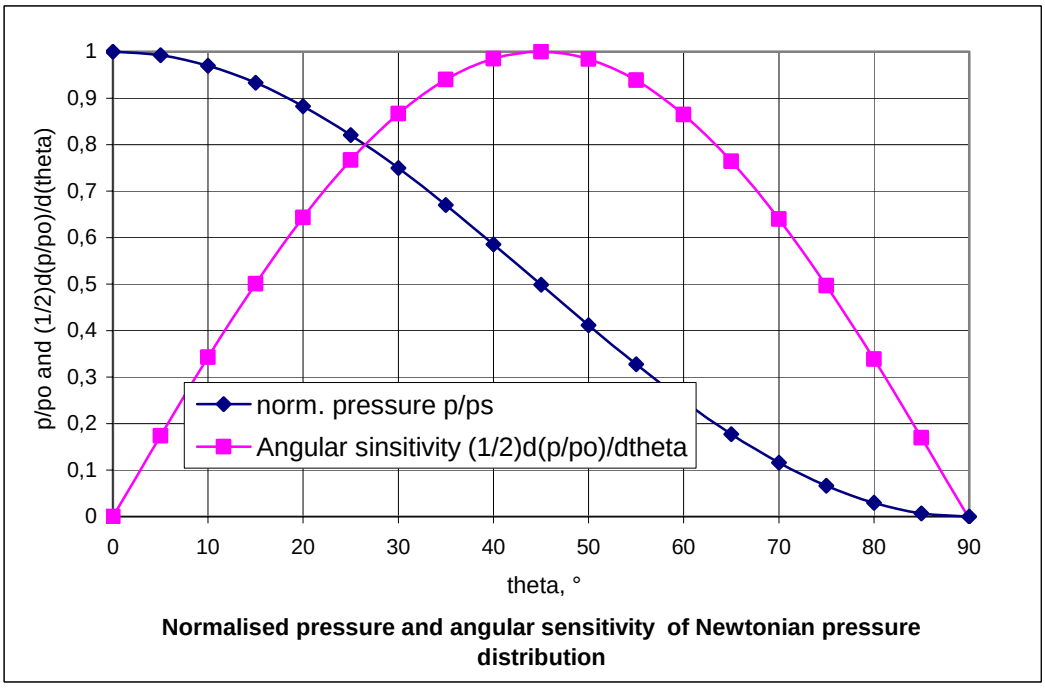

Fig. 7: Normalized Newtonian pressure distribution and angular sensitivity for one pressure tap

The relative angle of attack error is obtained by logarithmic differentiation of the probe function $p_{3-1} / p_0 = 4\sin^2 45° \cdot \tan\alpha$. At small angle of attacks α <10° (with sin α ~ α and cos α ~1) we obtain:

$$\left|\frac{\Delta\alpha}{\alpha}\right| = \left|\frac{\Delta p_{1-3}}{p_{1-3}}\right| + \left|\frac{\Delta p_0}{p_0}\right|$$

This means if we measure both pressures p_0 and p_{3-1} with an accuracy of 1% the resulting angle of attack accuracy will be 2% of alpha value.
It should however be noted that this analysis applies only if we have identical Newton factor k_N between the different pressure taps.
Real gas effects may influence the Newton factors between tap 0 taps 31 which would result in Newton factors of k_{N0} and k_{N13}.In this case the error formula would contain the following additional term:

$$\left|\frac{\Delta\alpha}{\alpha}\right| = \left|\frac{\Delta p_{1-3}}{p_{1-3}}\right| + \left|\frac{\Delta p_0}{p_0}\right| + \left|\frac{\Delta K_N}{K_N}\right|$$

4. Simple tools for pressure and heat load dimensioning of sensor heads

Principal tasks of the dimensioning are:

- Determination of the pressure measurement range for each sensor head.
- Determination of heat load measurement range for calorimetric sensor heads.
- Thermal dimensioning to withstand the maximum heat load and the time integrated heat load during the mission.

Fast engineering analysis methods are extremely useful for the dimensioning during the design phase. Simple ballistic trajectory analysis codes like the Allen-Eggers [8] or Chapman's method [9] combined analytical pressure and heat flux formula allow a fast analysis of the pressure, heat load and thermal response of the sensor heads along the complete trajectory. HTG relies on Allen Egger' entry dynamics combined with modified Newtonian surface pressure analysis and Lees [10] heat flux analysis.
As typical analysis example we show in Fig. 8 the dynamic pressure and velocity for the re-entry trajectory case B of the EXPERT vehicle [2]. In Fig. 9 we show as function of entry time the stagnation point heat flux and the resulting temperature of a calorimetric heat flux sensor of the RAFLEX type [11]. It should be noted that the thermal design of sensor heads has to consider both the maximum heat load during re-entry and the time integrated heat load during the whole re-entry phase. In the present analysis case the copper sensor head reaches a maximum temperature of 1300 K, which is only 60° below the melting temperature of 1360 K. Thus the calorimetric constant of the head has to be increased.

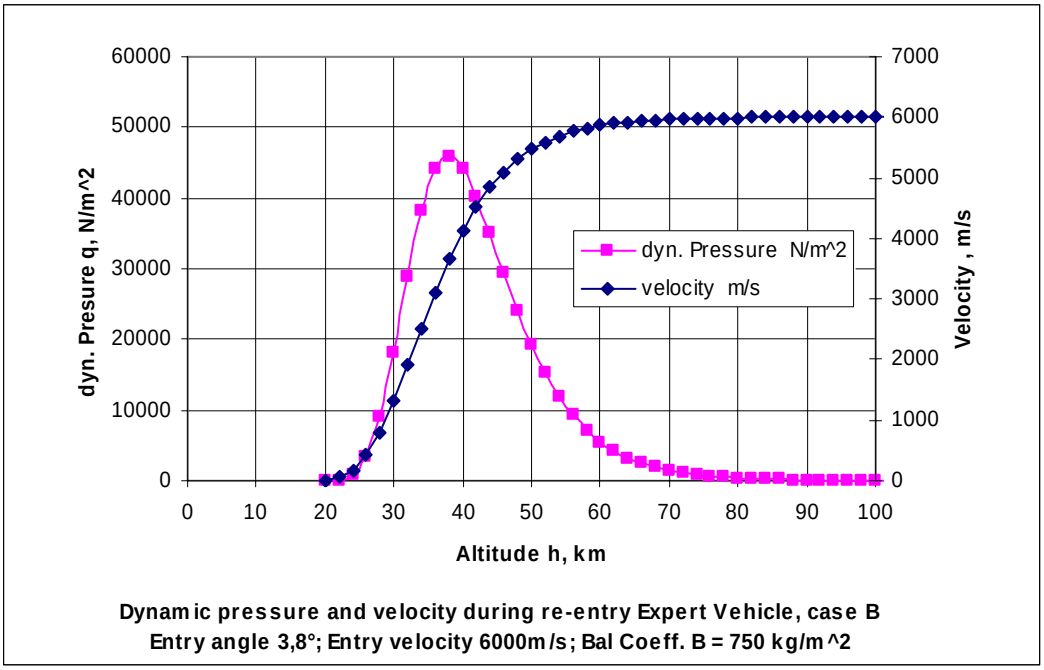

Fig. 8: Dynamic pressure and velocity EXPERT Case B, Sensor length 30 mm, B = 750 kg/m^2, entry angle = 3.8°

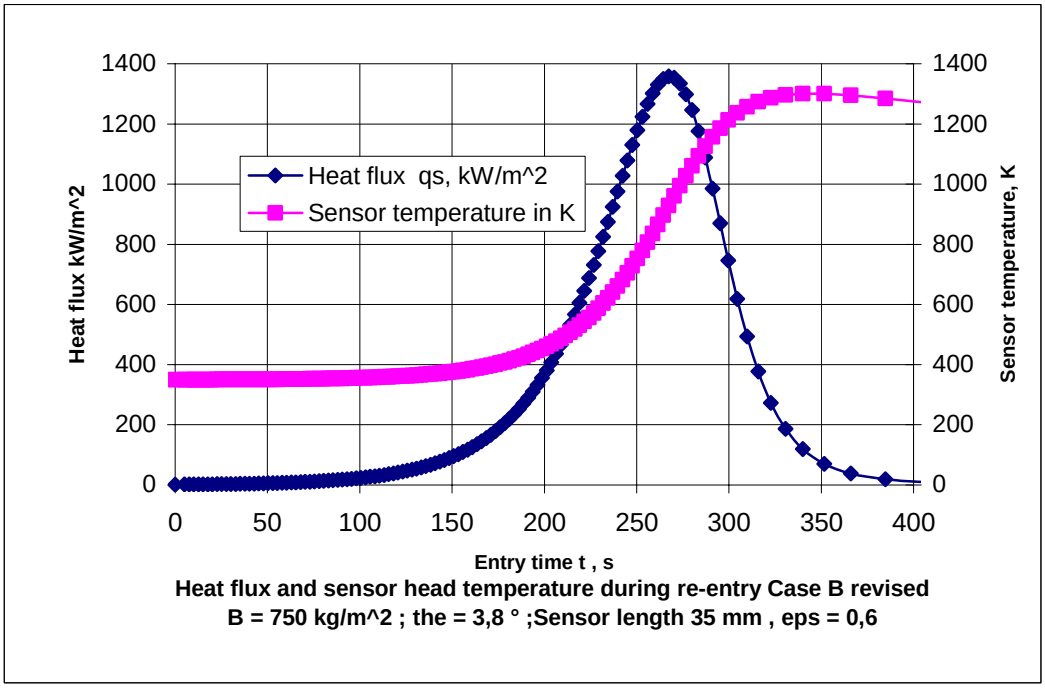

Fig. 9 Heat flux and sensor head temperature, EXPERT Case B, Sensor length 30 mm; B = 750 kg/m^2, entry angle = 3.8°

5 Some typical air data systems for re-entry vehicles

Typical air data systems used in re-entry vehicles are shortly summarized in the following.

5.1 The Shuttle Entry Air Data System SDS

The US Shuttle Entry Air Data System SEADS [12] consists of 14 nose cap orifices and 6 static orifices mounted behind the nose cap with smaller local surface inclination. Due to the asymmetric nose and due to safety considerations more than 5 pressure orifices had to be used. Therefore also the derivation of probe functions required a large computational and experimental effort. In order to cover the complete altitude range below 90 km each orifice is connected to a pair of 2 absolute pressure transducers with different measurement range. Fig. 10 shows a sketch of the Shuttle nose with the installation locations of the 20 probes.

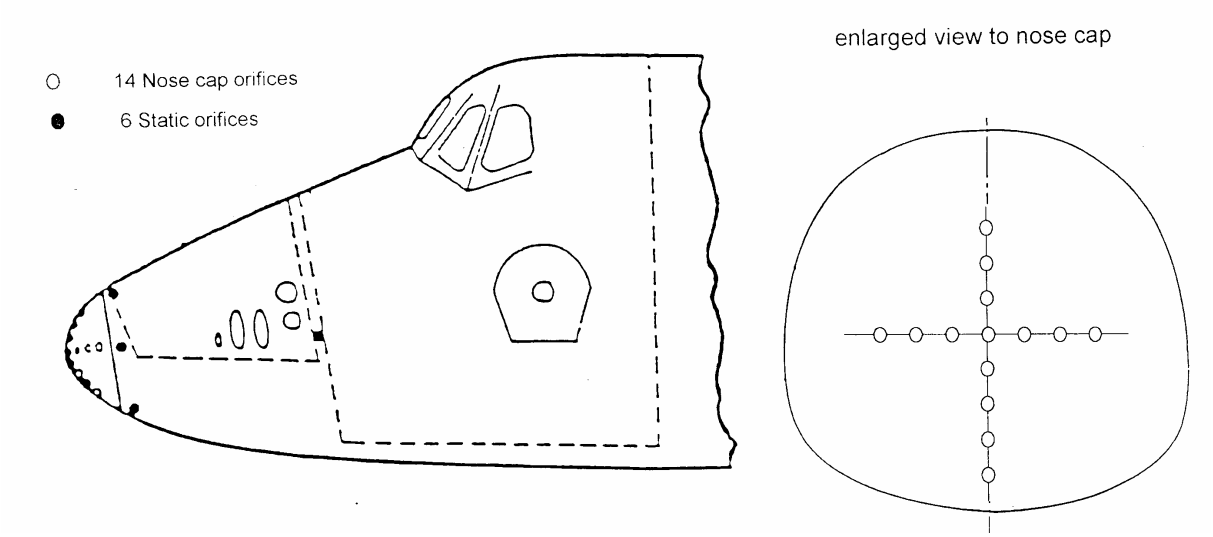

Fig. 10: Principle of Shuttle Entry Air Data system SEADS

5.2 The ARD capsule

The ARD capsule, whose geometry is shown in Fig. 11, has the Apollo shape and its spherical front part consists of a spherical segment with 22.6° half angle.
This means that the maximum pressure variation amounts on the flow exposed spherical surface at $\alpha = 0°$ is only to 15% and at $\alpha = 15°$ the pressure variation increases to 36%. Thus the air data system principally operates in the low sensitivity regime of Fig. 7.

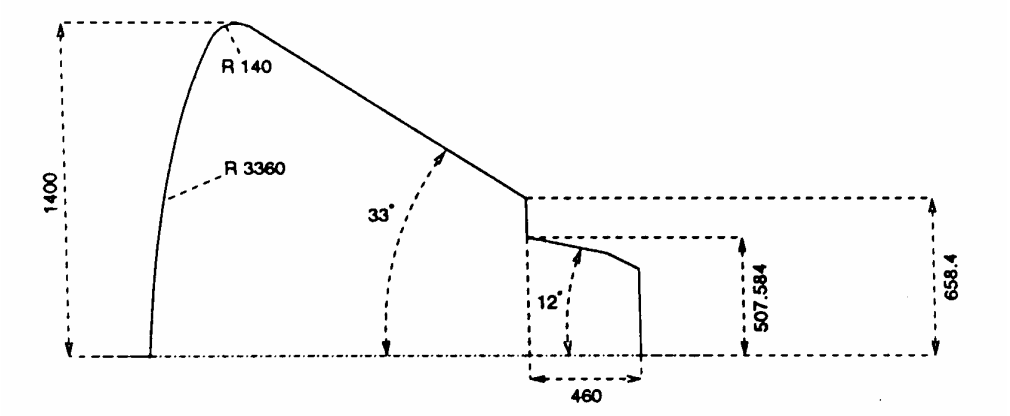

Fig. 11: Geometry of ARD capsule, dimensions in mm

5.3 The RAFLEX Air Data System and Instrumentation

The RAFLEX air data system (Re-entry Aerodynamic FLow Experiment) consists of combined flux probes measuring both pressure and heat flux. Up to now RAFLEX served for 3 entry capsules as air data system [11].

RAFLEX for Express Capsule

RAFLEX development started during the years 1993 – 1995 for the EXPRESS mission [13], [14]. The shape and the main dimensions of the EXPRESS capsule and sensor installation positions are shown in Fig. 12.

EXPRESS was launched in January 1995 and recovered after a launch failure and an unexpected recovery in Ghana in the middle of 1996. Due to these circumstances no flight data were obtained during the uncontrolled re entry. Inspection and calibration checks after landing showed that the hardware and sensors suffered no mayor damage due to the re-entry forces and heat loads.

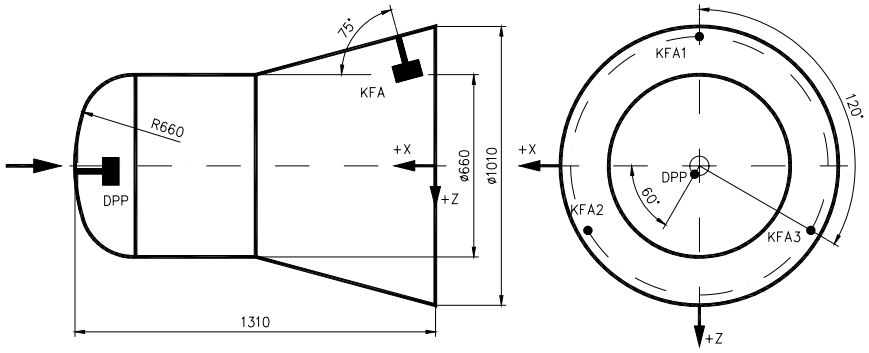

Sensor type	Measurement task
1 DPP Dynamic Pressure Probe	Free stream dynamic pressure
3 CFP Combined Flux Probe (KFA)	Particle flux, Slip flow, Heat flux Pressure (momentum flux) Combin. 1+2+3 → free stream orientation

Fig. 12: Raflex installation on Express Capsule

RAFLEX on MIRKA

MIRKA [15] was a ballistic re-entry capsule with a spherical shape of about 1m diameter and a total mass of 154 kg. (Fig.13), it was launched and recovered after parachute landing in October 1997. For MIRKA a second improved version of RAFLEX was developed. Excellent flight data were obtained during the re-entry.

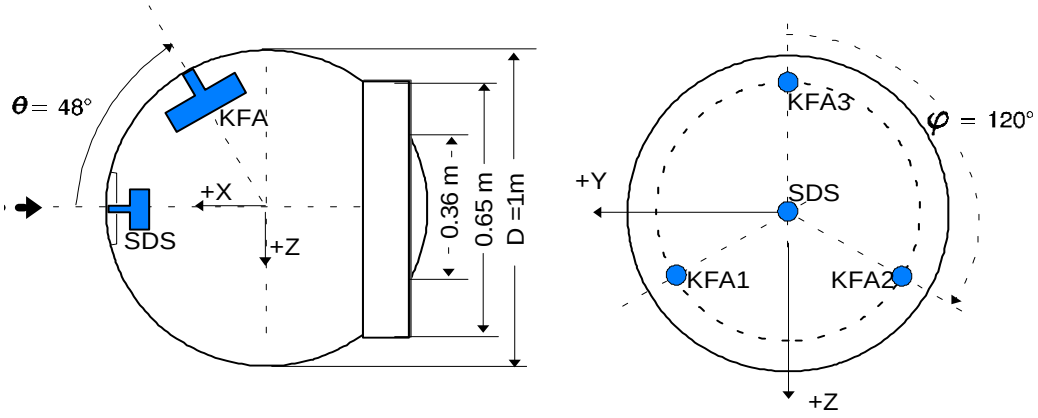

Sensor type	Measurement task
1 SDS Dyn. Pressure Probe	Free stream dynamic pressure
3 CFP (KFA) Combined Flux Probes	Heat flux Pressure (normal momentum flux) Combin. 1+2+3 → free stream orientation

Fig. 13: Geometry of MIRKA Capsule with sensor locations

RAFLEX on IRDT

IRDT (Inflatable Re-entry and Descent Technology) is a ballistic re-entry capsule with a two staged Inflatable Braking Unit (IBU) [11], [16]. Fig.14 shows the rigid part of the IRDT2 capsule with RAFLEX probe positions and the launch configuration with stowed IBU. The first IBU will be inflated at the beginning of the re-entry in an altitude of about 100 km while the second IBU acts as a parachute for landing.
In total one DSP (Dynamic Stagnation Point Probe), four CFP (Combined Flux Probe) and one BPP (Base Pressure Probe) were installed. DSP and CFP are capable of measuring heat flux and pressure. For DSP and CFP probes differential pressure transducers were installed obtaining the reference form the vehicle base. Therefore bas pressure was monitored with one absolute transducer. Due to an unfortunate launch failure no re-entry data could be obtained. Also IRDT was not recovered after an uncontrolled re-entry.

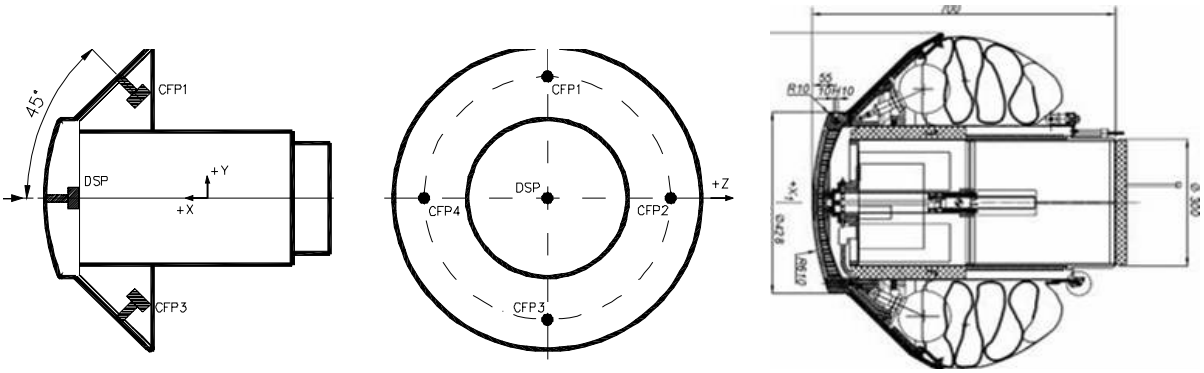

Sensor type	Measurement task
1 DSP Dynamic Stagnation Point Probe	Free stream dynamic pressure Stagnation Point heat flux
4 CFP Combined Flux Probes	Heat flux Pressure (normal momentum flux) Combin. 1+2+3 +4 → free stream orientation
1 BPP Base Pressure Probe	Base Pressure, reference pressure for CFP

Fig. 14: Geometry of IRDT rigid part with Raflex probe positions and IRDT with stowed IBU

6. RAFLEX design principles

The design and development of each RAFLEX system was dominated by the mission specific design loads, by the vehicle geometry, by the vehicle mechanical and thermal structure by the local installation position and by the restrictions imposed by other experiments.
For each new re-entry mission the RAFLEX system needed a redesign for the mechanical and thermal hardware as well as for the electronic parts of the sensor package. The basic principle of our combined flux probes remained however identical.

6.1 The basic principle of RAFLEX of combined sensor heads

The RAFLEX combined sensor heads measure with on head local simultaneously pressure and heat flux .The heat load sensor is based on the calorimetric principle. This means that the heat load acting on the sensor is stored by the calorimetric sensor head. The calorimetric sensor head has in addition a pressure tap which allows pressure and heat flux measurement at identical location. Sensor heads of this type can also be used in the rarefied slip flow regime were thermal transpiration influences the sensed pressure. Fig. 15 shows a principle sketch of a combined probe.

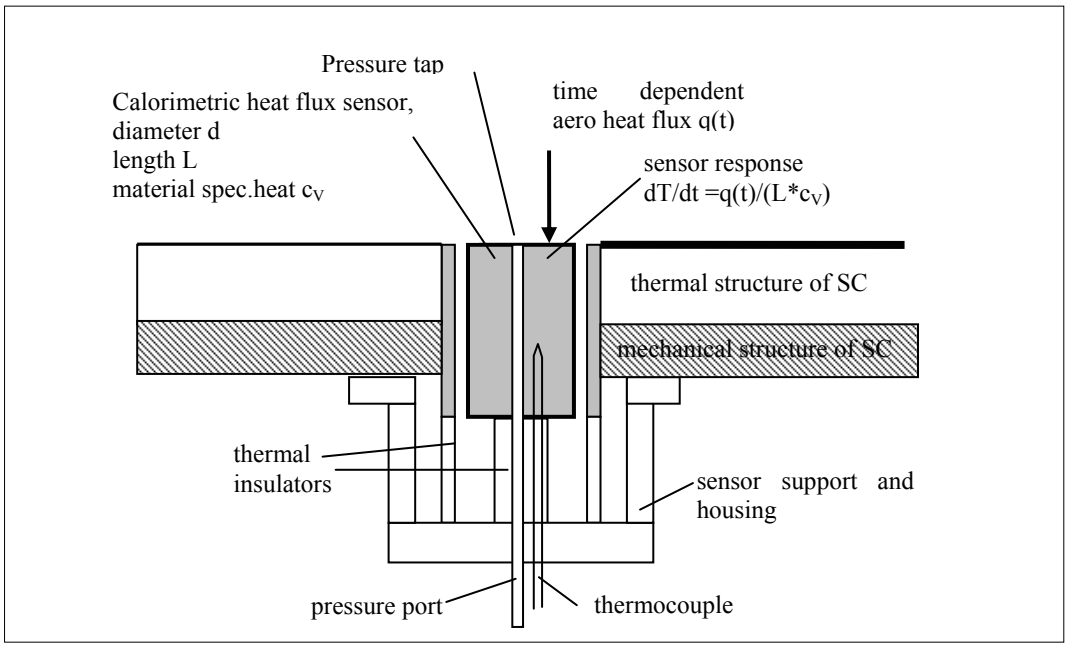

Fig. 15: Principle of combined RAFLEX sensor head for pressure and heat flux

As this head has also heat losses due to radiation and conduction the following simplified heat balance applies for a cylindrical calorimeter.

$$q'_{aer}\, A_{Sens} = H_C \frac{dT}{dt} + A_{Sens}\varepsilon\sigma T^4 + A_{Sens} k\left(T - T_{amb}\right)$$

with A_{sens} the flow exposed area of sensor head.

For a cylindrical calorimeter as sketched in Fig. 15 we obtain:

Sensing area: $A_{sens} = \frac{\pi}{4} d^2$ [m²]

Sensor heat capacity H_C: $H_C = c_V \frac{\pi}{4} d^2 L$ [J/K]

Calorimeter constant C_C: $C_C = \frac{H_C}{A} = c_V L$ [J/(m2K)]

Neglecting heat conduction we obtain for a sensor exposed to aerodynamic heating and radiative heat loss the following simple expression.

$$q'_{aer} = c_V L \frac{dT}{dt} + \varepsilon \sigma T^4$$

With this equation the aerodynamic heating can be deduced from the sensor temperature-time derivative dT/dt with a correction for radiation losses. The above formulation treats the sensor head as a lumped mass with infinite heat capacity. This means that the heating dT/dt is uniform with in the sensor volume. This assumption is only valid in case the heat penetration time t_P through the sensor is smaller than a characteristic time for a heat flux change during the re-entry $t_P << t_q$.
The penetration time is given by Fourier number $Fo_L = 0.1$, which gives

$$t_p = 0.1 \cdot L^2 c \frac{V}{k}$$

The characteristic time for a heat flux change t_q is given by a change of re-entry heat flux q(t) by a factor 1/e.

$$\left| \frac{dq(t)}{dt} \right| t_q = \frac{q(t)}{e}$$

$$t_q = \frac{q(t)}{e} / \left| \frac{dq(t)}{dt} \right|$$

The material selection of the sensor head has to consider the following demands:

- High melting temperature
- High specific heat
- High heat conduction

In the following table we compare thermal properties of candidate materials.

Material	Density g/cm^3	c_M J/(g K)	c_V J/(cm^{3}K)	K J/cm s K)	a cm^2/s	T_{melt} K	t(Fo =0.1) for L= 1 cm Second
Copper	***8.96***	***0.396***	***3.53***	***3.84***	***1.18***	***1356***	***0.0847***
Silver	10.5	0.239	2.52	4.19	1.67	1235	0.0493
Gold	19.3	0.130	2.51	3.06	1.226	1336	0.0816
Nickel	8.9	0.444	3.95	0.623	0.158	1731	0.633
Titanium	4.5	0.523	2.35	0.219	0.093	1933	1.08
Molybdenum	10,22	0.251	2.56	1.38	0.539	2890	0.186

Table 3: Thermal data of candidate materials for calorimetric head

It is evident that copper has the best material properties. Sensor heads with 20mm length have a penetration time of 0.3 sec whereas characteristic times for heat load change are during the re-entry heating phase larger than tq > 10 sec. Thus an adequate time resolution can be achieved with this heads.

6.2 Mission specific design influence

Mission and trajectory dependent design influences are the maximum heat flux q'_{max} , the local heat flux profile q'(t) as function of re-entry time, its integral $Q = \int q'(t)dt$, the maximum dynamic pressure q_{max} and the pressure profile p(t). This quantities influence primarily the sensor head dimensioning and the range of pressure transducers.
With the given data for a new mission, like capsule shape and mass, re-entry trajectory and location for the sensor installation in the capsule, we evaluated the heat flux and pressure profiles over the flight time.
In the next table the maximum stagnation point heat flux and dynamic pressures are shown for the three RAFLEX missions. Express capsule had an extreme high ballistic coefficient B and had thus a low altitude re-entry trajectory, whereas the inflatable demonstrator IRDT re-entered at high altitudes.

Mission	**Ball. Coefficient $B=m/C_D*A$**	**Altitude h max. deceler.**	**Max.heat flux stagnation point**	**Max. dynamic pressure**
	kg/m^2	Km	[kW/m²]	[mbar]
EXPRESS	972	37,7	3000	2000
MIRKA	200	52	2000	500
IRDT2	36	68	800	150

Table 4: Mission and trajectory specific design loads

The design values for the RAFLEX sensors had to be based on heat flux and pressure on local installation position. These values are shown in the next Table.

Mission	**Installation position**	**Design heat flux**	**Calorimeter dimensions**	**Peak dyn. Pressure**	**Pressure Transducer**
		[kW/m²]	∅·L [mm]	mbar	mbar
EXPRESS	Stagn. Point	3000	-	2000	3000 1000
	Conical Flare	600	∅16 x 30		1000 abs. 10 abs. 10 diff.
MIRKA	Stagn. Point	2000	-	500	1000 abs. 10 abs.
	48°-position	1200	∅10 x 40		1000 abs. 10 abs.
IRDT2	Stag. point	800	∅10 x 30	150	330 diff.
	Cone	400	∅10 x 16		330 diff.

Table 5: Design values for heat flux sensor heads and pressure transducer range

In the EXPRESS and MIRKA capsule we had limited access to the stagnation point and therefore only pressure sensing ports could be installed. As port materials were used SIC In the EXPRESS capsule and TZM (a molybdenum alloy) in the MIRKA capsule.

6.3 The influence of vehicle mechanical and thermal structure

The principal dimensioning of heat load sensors and pressure transducer can in principle be performed without knowledge of local vehicle structure. The local structure of the vehicle has however dominant influence of on the final design of a probe.
As explained in the following table each probe assembly consists of the 4 basic components each with specific tasks.
The sensor housing with mounting socket is the primary interface to the vehicles mechanical and thermal structure. The mounting socket has to compensate the hazardousness which results from putting holes into the external thermal and internal mechanical structure of the vehicle.
The design of the mounting depends therefore completely on the local vehicle structure. MIRKA and IRDT are demonstrative examples for complex and simple installations.

Component	Tasks
Sensor head	Primary sensing on vehicle surface Transmission to sensing instrument Thermal insulation between surface and inside
Sensor housing with mounting unit	Main interface to vehicle structure Support of sensor head Support for transducers Support for electrical sockets Pressure sealing between out - inside Compensation of differ. thermal expansion Thermal insulation
Sensing instruments (pressure transducers, thermocouples)	Transformation of primary quantity in electrical signal
Electrical sockets and lines	Connection to power supply and data acquisition system

Table 6: Probe components and specific tasks

RAFLEX II installation in MIRKA

The double wall structure of MIRKA with RAFLEX installation is shown in Fig. 16. Within the MIRKA double walled structure a surface protected ablator SPA is located. The ablator is covered by the thin outer skin made of C/SIC, and the inner load carrying structure is made of CFRP. The ablator is positioned in a honey comb like structure, which allows the ablating gases to flow to the base where they are discharged, Fig. 16 shows that a very complex installation design of RAFLEX sensors was necessary. The installation had to provide sealing between outside and ablating room and sealing between ablating room and the vehicle inside. The installation had in addition to compensate various thermal expansions.

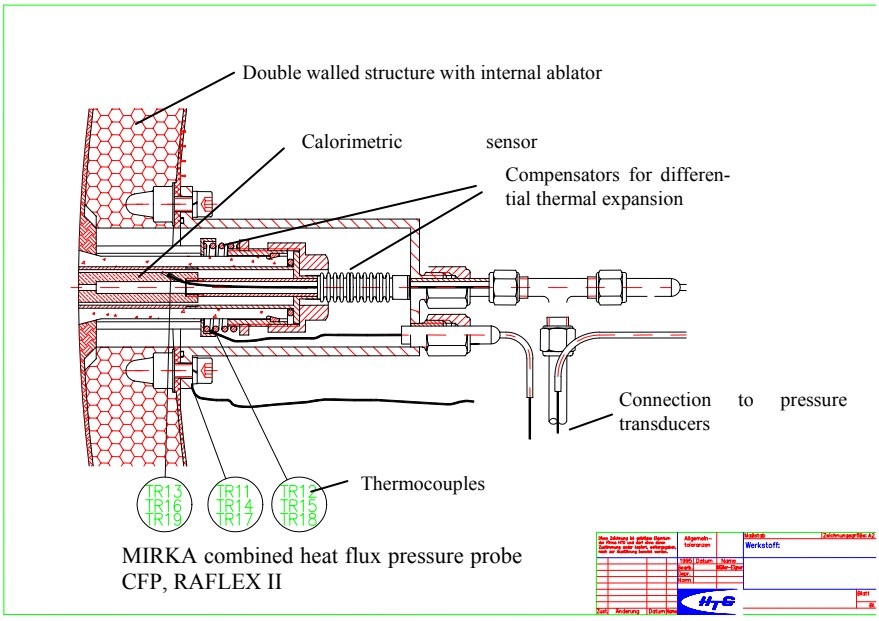

Fig. 16: RAFLEX II combined flux probe installation in MIRKA

RAFLEX III installation on IRDT

The rigid part of the IRDT capsule consists of a load bearing aluminum shell covered with ablator. At each installation location of a Raflex Probe the ablator was replaced by ceramic tile with 100 mm diameter. Thus the REFLEX III had only to pass through the aluminum shell the ceramic tile. Fig. 17 shows the installation detail.

Due to experience gained with MIRKA smaller pressure transducers were selected and the total mass of one probe unit could be reduced from 1800 grams at MIRKA to 500 grams.

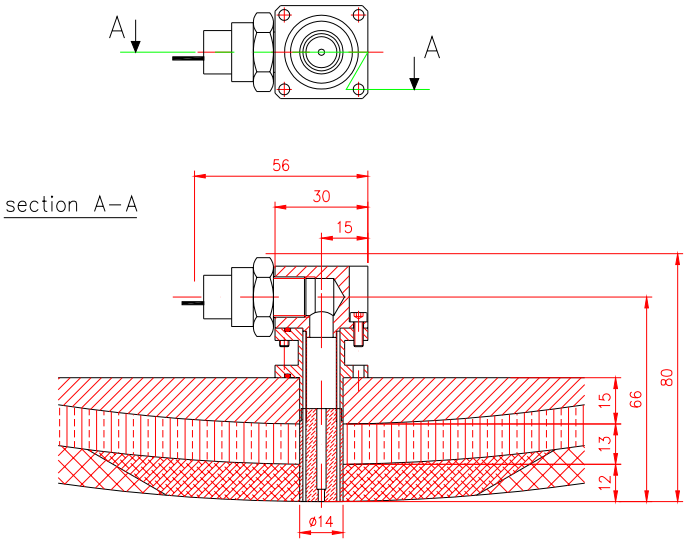

Fig.17: Installation drawing of RAFLEX III in stagnation point of IRDT

7. Electronic components and mass budget

The following table shows as example the electrical supply and output data of RAFLEX III on IRDT.

	Supply Voltage	Current	Output Voltage
DPP Dyn. pressure probe	± 15 V	15 mA	0-10 V
CFP 1Static probe	± 15 V	15 mA	0-10 V
CFP 2 Static probe	± 15 V	15 mA	0-10 V
CFP 3 Static probe CFP	± 15 V	15 mA	0-10 V
CFP 4 Static probe CFP	± 15 V	15 mA	0-10 V
Thermocouples	0		
2 DPP, Type K			0- 50 mV
8 CFP1-CFP4 Type K			0-50 mV
Total	5* ± 15 V 5 supply lines	75 mA	 15 output lines

Table 7: Electrical supply and output data of RAFLEX III

Power supply for sensors and acquisition of these data can either be provided by a central on board unit or by a experiment dedicated separate unit. We usually us for each pressure signal a scan rate of 30 HZ and for temperatures scan rates of 3-5 Hz.

Typical mass budget of air data system

Typical for the mass of 5 probe air data system may be the mass budget of the HTG RAFLEX III system mounted on IRDT2. The detailed component data are given in the following table.

Component	Mass (Total/Component)		Explanation	Type of Interface
Dyn. pressure probe	390 g			
Sensor head with mounting unit		200 g	Head for pressure and calorimeter	Mechanical. and thermal structure
Pressure Transducer with signal conditioner		110 g		Electric
Thermocouples		30 g	3 Thermocouples	Electric
Local harness		50 g		
4 Combined flux probes	1360 g			
Sensor head with mounting unit		150 g	Head for pressure and calorimeter	Mechanical. and thermal structure
Pressure Transducer with signal conditioner		110 g		Electric
Thermocouples		30 g	3 Thermocouples	Electric
Local harness		50 g		
Total mass	**1750 g**			

Table 8: Mass budget RAFLEX III air data system for pressure heat flux measurement

It also should be remembered that in the instrumentation mass budget the contributions of electrical wiring, which establish connection to the data logger, can not be neglected.

8. Validation and qualification testing of the probes

Validation and qualification testing shall assure the correct operation of a measurement system during flight operation. In principle we distinguish between the testing on the component and on the system level. As demonstrative examples for the different activities we use our RAFLEX system.

Calibration tests of sensors
Calibration test of sensors are usually conducted at simulated vacuum and pressure conditions during the development and before delivery of an instrumentation system. These tests also serve to identify appropriate transducers and electronic equipment

Wind tunnel tests for determination of sensor functions
Wind tunnel tests are usually necessary to validate the numerically derived sensor functions. Therefore either a complete model of the vehicle or a model of the vehicle nose section instrumented with pressure ports and pressure sensors will be required.
Fig. 18 shows the rigid nose part of the IRDT capsule during a wind tunnel test at Ma = 9 in our HHK facility.

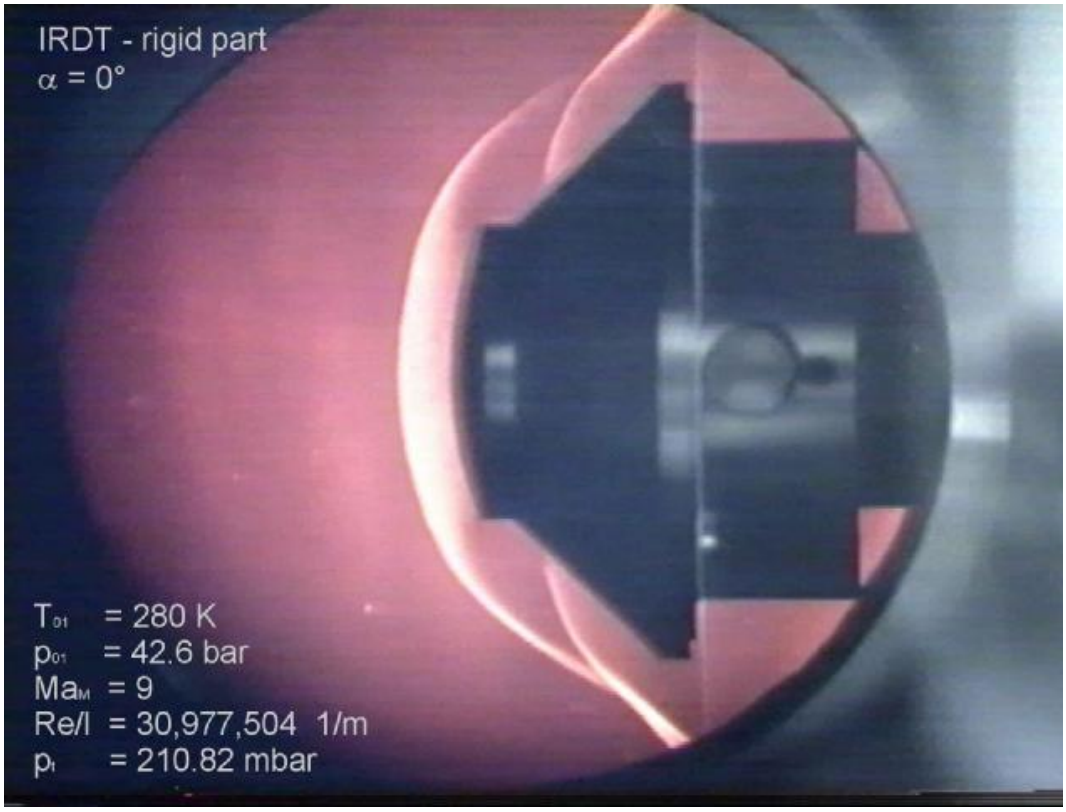

Fig. 18: Schlieren picture of IRDT2 model in HHK win tunnel at Ma= 9

Heat load testing

Heat load testing is part of the flight qualification for a re-entry experiment. A complete probe unit mounted in a simulated installation environment has to be tested. During these tests the actual heat load and pressure profile during re-entry shall be duplicated in a ground facility. These types of tests we had to conduct for each of our 3 RAFLEX systems. As the flight dependent time profile of q' is difficult to simulate the model is usually tested with maximum heat load q'_{max} for a time period, which assures that also the time integral of heat load is simulated. Fig. 19 shows the e IRDT RAFLEX III stagnation point probe after the heat load test in a Plasma Jet Facility (U-13UHFP at Babakin).

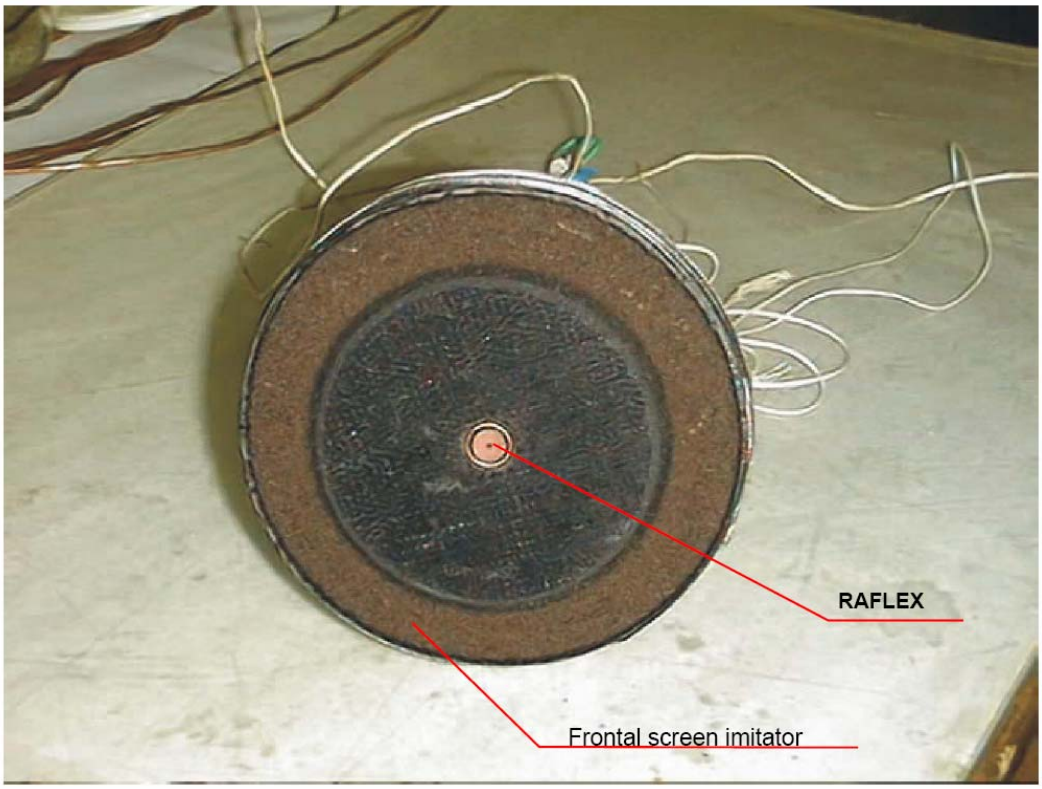

Fig. 19: IRDT2 RAFLEX III stagnation point probe after the heat load testing

Vibration testing

Vibration testing is also part of the instrument qualification and is usually conducted on the subsystem and on completes system level. The test have to demonstrate that the instrument payload will accept the dynamic launch loads and that the instrument will not damage the vehicle. It should be noted that vibration tests show often unexpected failure of sensitive mechanical components.

9. Some flight results with RAFLEX system

RAFLEX I on EXPRESS

Due to the start failure EXPRESS didn't reach the nominal orbit and the experiments could not be activated. EXPRESS capsule re-entered uncontrolled after some orbits and was one year after launch recovered in Ghana in the middle of 1996. We thus were able to recover also our RAFLEX sensor system. The instrumentation showed no damage due to re-entry forces and heat loads. Even a re-calibration of the pressure transducers was possible. Thus EXPESS was partially successful for direct flight qualification of our system

RAFLEX II on MIRKA

MIRKA was launched on October 9, 1997 together with the Russian FOTON-11 by a SOJUS rocket from Plesetsk. After 14 days in orbit MIRKA the successful re-entry of MIRKA was initiated with a final parachute landing in Kazakhstan on October 23, 1997. Our RAFLEX system worked during the whole re-entry successfully. Fig. 20 shows a combined flux probe sensor head after the re-entry mission.

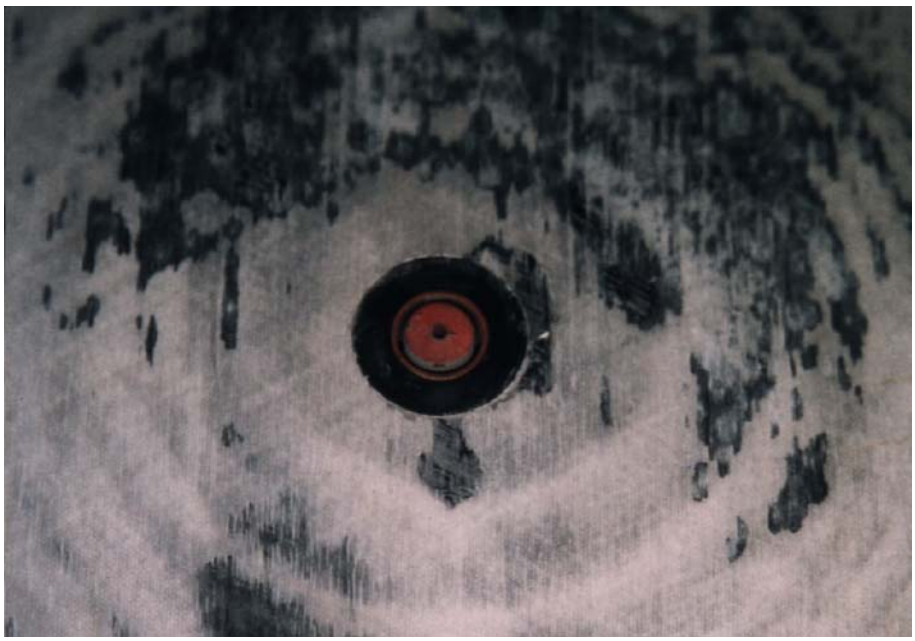

Fig 20: RAFLEX II sensor head after MIRKA re-entry

Fig. 21 shows the recorded pressures of the 4 Raflex probes during the complete re-entry, which covered a time span from 1150 to 1500 seconds. A detailed evaluation of the pressure oscillations for the period between 1300-1320 seconds is shown in Fig. 22.
An evaluation of this data showed that MIRCA conducted a coning motion which is shown in an alpha – beta plane of Fig. 23 for a period of 6 seconds. This example demonstrates the high time resolution of the RAFEX II air data system.

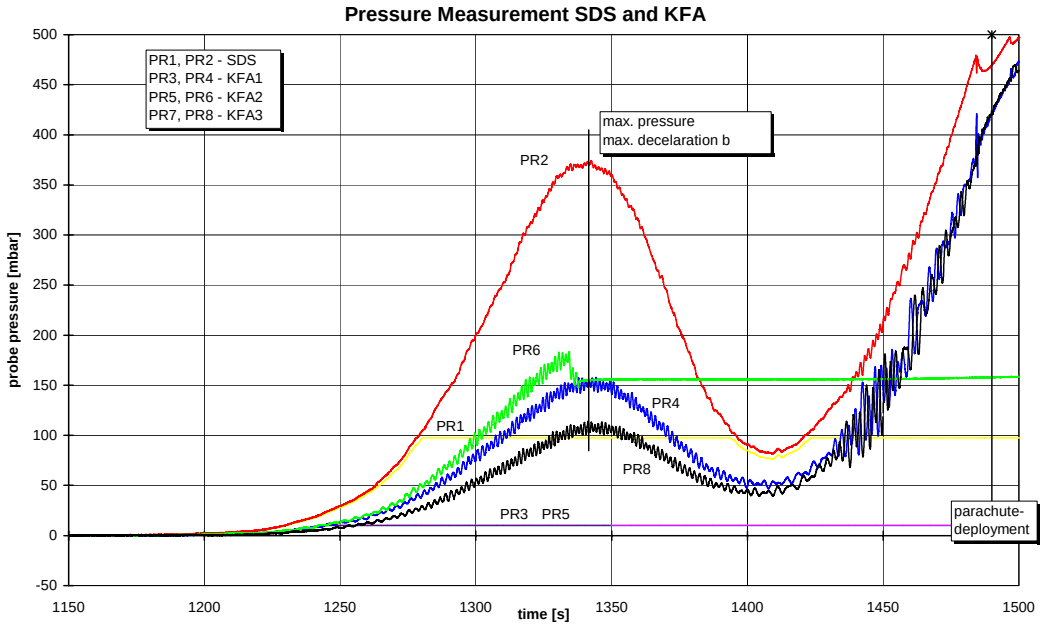

Fig. 21: Recorded RAFLEX pressure during MIRKA re-entry

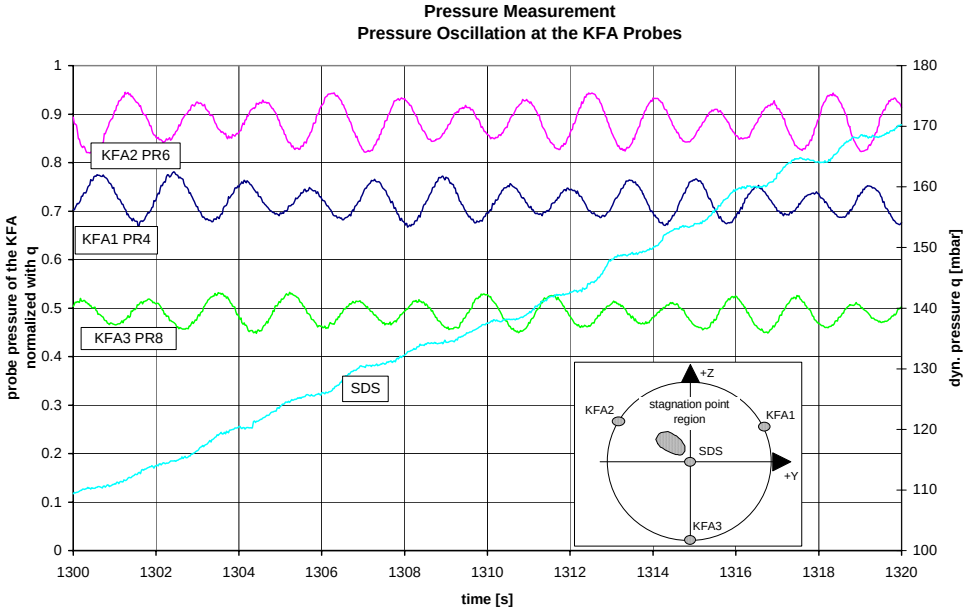

Fig 22: Evaluated RAFLEX pressure during 20 s time period, t=1300-1320s

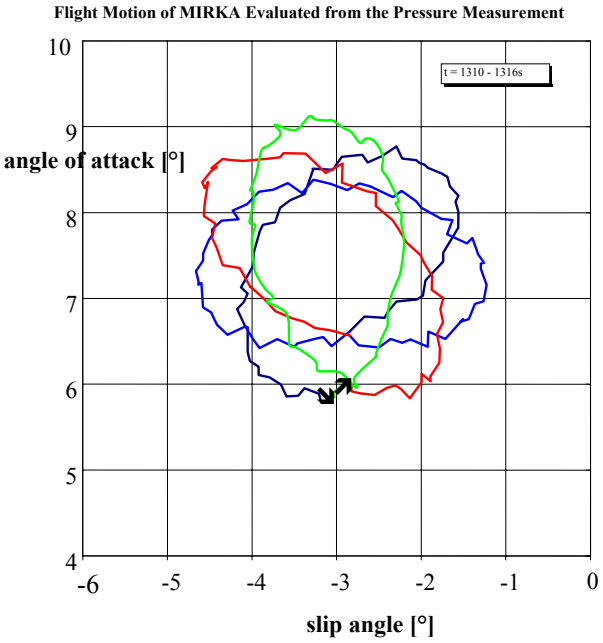

Fig. 23: MIRKA re-entry, angle of attack versus slip angle, t = 1310-1316s

10. Conclusions

The complete development process for hypersonic air data systems and for heat flux probes has been outlined on basis of RAFLEX installed in 3 different re-entry capsules.
The experience showed that for each re-entry vehicle a new design was required by mission and vehicle structure.
Thus for each new type of re-entry vehicle a dedicated development and design of air data system seems necessary.
Only the experience, the basic design methodology and some identical type of mechanical and electronic parts may be used on different projects.

Literature

[1] G. Koppenwallner
Definition of requirements and operational specifications for FADS
WP1 Report, Flush and Laser Air Data System
HTG TN-03-6, 2003

[2] L. Walpot, H. Ottens
FESART/EXPERT Aerodynamic and Aerothermodynamic Analysis of the REV and KHEOPS Configuration
ESTEC TN TOS-MPA/2718/LW

[3] Liepmann H. W. Rhosko
Elements of Gas Dynamics
John Wiley, New York 1957

[4] Lewis C. H., Burgess III E.G.
Altitude velocity table and charts for imperfect air
AEDC–TDR-64-214, 1965

[5] Anonym
Atmospheric and Space Flight Vehicle Coordinate Systems
AIAA recommended Practice
ANSI/AIAA R-004-1992

[6] W.R. Wells; W.O. Armstrong
Tables of aerodynamic coefficients obtained from developed Newtonian expressions for complete and partial conic and spherical bodies at combined angles of attack and sideslip
NASA TR R-127

[7] Häuser J. Dai Wuye
Numerical Simulation for the Flush and LASER air Data System
WP3 Report, Flush and Laser Air Data System
CLE, Salzgitter, Germany 2004

[8] Allen.H. J.; Eggers,jr. A. J.
A study of the motion and aerodynamic Heating of Missiles entering the Earth's Atmosphere at High Supersonic Speeds
NACA TN- 4047, Washington USA, 1957

[9] Chapman D. R.
An approximate analytical method for studying entry into planetary atmospheres
NACA TN 4276, Washington 1958, and NASA TR-11, Washington 1959

[10] Lees, Lester
Laminar Heat Transfer over Blunt –Nosed Bodies at Hypersonic Speeds.
Jet Propulsion Vol. 26, No. 4, 1956, pp. 259-269

[11] R. Müller Eigner, G. Koppenwallner
RAFLEX an Air Data System for Re-entry Vehicles
4th European Symposium on Aerothermodynamics for Space Vehicles
ESA SP 4876, 2002, pp. 457-464

[12] Cunningham J.A. et al.
Shuttle Entry Air Data System, Pre-flight Testing and Analysis
AIAA Journal of Spacecraft, Vol. 24, No. 1, 1987, pp. 33-39

[13] G. Koppenwallner, D. Johannsmeier, R. Müller Eigner
High altitude free flight experiments and instrumentation developed for Brem-SAT and Express capsule
2nd European Symposium on Aerothermodynamics of Space Vehicles
ESA SP 358, 1995, pp. 437- 444

[14] Auweter-Kurtz M., Hald H., Koppenwallner, G., Speckmann, H.-D.
"German Re-entry Experiments on EXPRESS"
IAF-94-1.3.192, 45th Congress of the International Astronautical Federation, Israel, 1994

[15] R. Müller Eigner, G. Koppenwallner
Pressure and Heat Flux Measurement with RAFLEX 2 during MIRKA Re-Entry
3rd European Symposium on Aerothermodynamics of Space Vehicles
ESA SP 426, 1999, pp. 685-689

[16] R. Müller-Eigner
Instrumentierung der IRDT2 Kapsel mit RAFLEX III
Abschlußbericht des Zuwendungsbescheids 50 JR 0082
HTG-Report 04-01, HTG 2004